Structure design of a 2-D high-aspect-ratio resonant microbeam accelerometer

Deng-Huei Hwang
NeoStones Microfabrication Corporation
Research and Development Center
HsinChu, Taiwan
E-mail: a1004@neostones.com.tw

Kan-Ping Chin
National Chiao Tung University
Department of Mechanical Engineering
Taiwan

Yi-Chung Lo
National Synchrotron Radiation Research Center
HsinChu, 30077, Taiwan

Wensyang Hsu
National Chiao Tung University
Department of Mechanical Engineering
Taiwan

Abstract. An accelerometer with concise structure having a resonant microbeam to measure 2-D acceleration is proposed. This structure is configured with a central proof mass suspended by four symmetrical and orthogonal high-aspect-ratio (HAR) microbeams. This dual-axis design is able to decouple a two-axis signal from a 2-D acceleration. An analytical model relating the linear relationship between the acceleration and the associated resonant frequency shift of microbeam is derived, and a finite element analysis (FEA) is also performed to confirm this model. The FEA result also shows that there is little cross talk between *x* and *y* directions of measurement, meaning that this structure is able to decouple a planar 2-D acceleration into two independent acceleration components, and therefore the 1-D analytical model can be used to evaluate the 2-D acceleration on the *x*-*y* plane. In addition, the model is verified by testing results of one conventional dual-axis natural frequency shifted microaccelerometer (DFSM). The simulation result also shows that the sensitivity of the proposed HAR accelerometer is triple that of a conventional DFSM.
 [DOI: 10.1117/1.2037070]

Subject terms: resonant; accelerometer; frequency shift; high aspect ratio; decouple; cross talk.

Paper 04157RR received Nov. 15, 2004; revised manuscript received Feb. 23, 2005; accepted for publication Feb. 25, 2005; published online Aug. 19, 2005.

1 Introduction

Due to remarkable sensitivity and linear response, many microsensors based on the frequency shift principle have been developed, including microaccelerometers.[1–8] In these accelerometers, the resonant frequency of the accelerometer structure or its substructure, e.g., vibrating beam, will be shifted by the variations of structure strain, stress,[1–6] or rigidity.[7,8] However, most of the previous microaccelerometers using the frequency shift principle were only capable of measuring 1-D acceleration, except Chang's design,[6] a dual-axis natural frequency shifted microaccelerometer (DFSM), which could successfully decouple a two-axis signal and detect 2-D acceleration. However, the rigidity of its microbridge fabricated by surface micromachining was too weak to resist deflection caused by the connected proof mass, and thus additional constraint bridges were required to support the proof mass, leading to a complex structure. This not only complicated the model derivation and fabrication process, but also reduced the acceleration measurement sensitivity. Also, due to the inherent limitation resulting from surface micromachining, the available area underneath the microbridge for forming capacitors to respectively drive and detect vibration was difficult to enlarge.

Here, a high-aspect-ratio (HAR) resonant microbeam accelerometer to detect a planar 2-D acceleration is proposed, which can be fabricated by various novel micromachining techniques, such as Deep Reactive Ion Etch (DRIE),[9] Lithographie Galvanoformung Abformung (LIGA),[10] and LIGA-like processes.[11–13] In contrast to the conventional DFSM design,[6] the proposed accelerometer is configured with a suspending proof mass supported by just four identical, orthogonal, and HAR microbeams, requiring no constraint bridges, since the HAR feature can enhance rigidity along the gravitational direction to support the proof mass without sacrificing the structural compliance in-plane. In addition, compared to the limited capacitor area formed underneath the supporting microbridges in conventional DFSM, the capacitors in the proposed design are placed at two sides of the microbeams; thus the area of the capacitors can be enlarged by the HAR structure. Also, a thicker and heavier proof mass can be obtained without using a complex leverage mechanism[1–3] to increase sensitivity.

An analytical model is first derived to relate the natural frequency shift of the microbeam and the applied acceleration by following the classic mechanics and vibration theory.[14,15] Finite element analysis (FEA) and experimental data from previous literature[6] are also used to confirm the analytical model and show the sensitivity improvement of the proposed design.

2 Structure Design and Operation Principle

The structure of the proposed high-aspect-ratio dual-axis frequency-shifted microaccelerometer is shown in Fig. 1. This microaccelerometer is operated using electrostatic force, and two respective electrode pads Gd and Gs adjacent to the two sidewalls of each microbeam are placed to form two capacitors to drive and sense the transverse vibration of the microbeams A, B, C, and D. To distinguish the

1537-1646/2005/$22.00

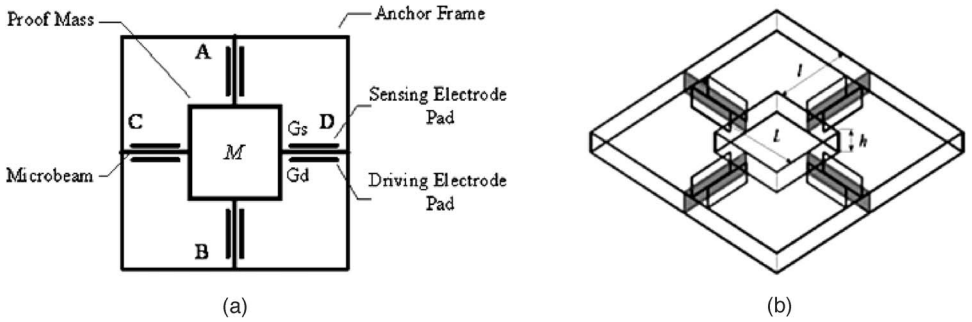

Fig. 1 The proposed HAR 2-D resonant microbeam accelerometer: (a) top view and (b) elevated view.

term of "microbridge" in conventional DFSM design,[6] "microbeam" is adopted here to describe the HAR beam in the current design with larger thickness.

Figure 2 shows the microaccelerometer under acceleration along the *y* direction. The inertial effect of the proof mass *M* applies a tensile and a compression on microbeams A and B, respectively, which shifts the natural frequencies of the two microbeams, as shown in Fig. 3. To detect such *y*-directional acceleration, the driving electrode pads Gd shown in Fig. 1 generate the variable electrostatic forces to respectively actuate microbeams A and B to vibrate at their natural frequencies.

On the other side, the sensing electrode pads Gs respectively sense the natural frequency variations of the excited microbeams A and B. Thus, if a relationship between the acceleration and the shifted natural frequency of the microbeam subject to the axial load is realized, the *y*-directional acceleration can be evaluated by the natural frequency shift. Similarly, the *x*-directional acceleration can also be evaluated in the same way using microbeams C and D.

3 Analytical Modeling

A model based on the Euler-Bernoulli beam theory is derived to estimate the natural frequency shift of the microbeam. Compared to the proof mass, the inertial effect of the microbeam is negligible, and thus is ignored in this derivation.

3.1 *Analytical Model of the Microbeam*

To estimate the frequency shift of the microbeams A, B, C, and D, as shown in Figs. 1 and 3, the continuous system theory in Ref. 14 depicting the transverse vibration of the elastic beam subject to an axial force *T*, with a clamped-clamped boundary condition, is used.

The governing equation is

$$EI\frac{\partial^4 y}{\partial x^4} + T\frac{\partial^2 y}{\partial x^2} + \rho A\frac{\partial^2 y}{\partial t^2} = 0. \tag{1}$$

The clamped-clamped boundary condition is expressed as

$$y(x,t)|_{x=0} = 0, \qquad \left.\frac{\partial y(x,t)}{\partial x}\right|_{x=0} = 0,$$

$$y(x,t)|_{x=l} = 0, \qquad \left.\frac{\partial y(x,t)}{\partial x}\right|_{x=l} = 0.$$

To evaluate the fundamental natural frequency of the microbeam, the assumed mode method is used to solve Eq. (1). The first mode shape function of the microbeam is derived and shown as

$$\phi_1 = C_1\cosh(a_n x) + C_2\sinh(a_n x) + C_3\cos(b_n x) + C_4\sin(b_n x), \tag{2}$$

where

$$a_n = \left(\frac{1}{2}\left\{-\frac{Tl^2}{EI} + \left[\left(\frac{Tl^2}{EI}\right)^2 + \frac{4m\omega_n^2 l^4}{EI}\right]^{1/2}\right\}\right)^{1/2}, \tag{3}$$

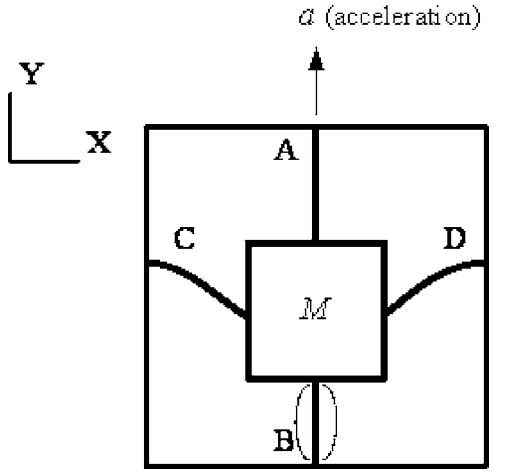

Fig. 2 The exaggerated deformation tendency of the microbeams due to *y*-directional acceleration.

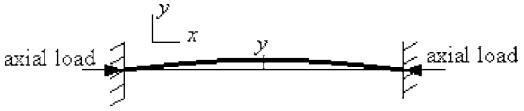

Fig. 3 The primary vibration mode of the clamped-clamped microbeam B subject to an axial load.

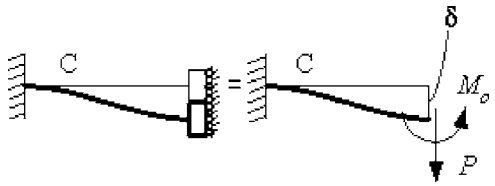

Fig. 4 The boundary of microbeam C comprising a fixed clamped end and a movable clamped end.

$$b_n = \left(\frac{1}{2}\left\{\frac{Tl^2}{EI} + \left[\left(\frac{Tl^2}{EI}\right)^2 + \frac{4m\omega_n^2 l^4}{EI}\right]^{1/2}\right\}\right)^{1/2}, \tag{4}$$

and $m=\rho A$.

By substituting the clamped-clamped boundary condition into Eq. (2) to solve the undetermined constant coefficients C_1, C_2, C_3, and C_4, the characteristic equation can be obtained as

$$(a_n^2 - b_n^2)\sinh(a_n)\sin(b_n) + 2a_n b_n[1 - \cosh(a_n)\cos(b_n)] = 0. \tag{5}$$

From Eq. (5), the shifted natural frequency of the microbeam subject to an axial load T can be calculated. However, when the axial load on the microbeam is zero, the fundamental natural frequency of the microbeam becomes

$$\omega_1 = 22.4\sqrt{\frac{EI}{ml^4}}. \tag{6}$$

3.2 *Load Analysis of Microbeams*

The boundary constraints of each microbeam A, B, C, or D can be considered as one end fixed on the anchor frame, and the other one clamped on the movable proof mass accelerated along the y direction, as shown in Fig. 4, by taking microbeam C as an example. It can be seen that the deflection on the movable clamped end of microbeam C is caused by a concentrated force P and a moment M_o at the end due to the proof mass under acceleration. Thus, the resultant deflection of the microbeam C due to the assumed concentrated force P, together with the moment loading M_o, is

$$\delta = \frac{Pl^3}{12EI}. \tag{7}$$

Based on the structural continuity, the bending deflections of microbeams C and D, as shown in Fig. 4, must equal the elongation of microbeam A and the shrinkage of microbeam B, respectively, due to the axial tension T_A and the compression T_B. Therefore,

$$\delta = \frac{T_A l}{EA} = -\frac{T_B l}{EA}. \tag{8}$$

As shown in Fig. 5, in equilibrium, the forces P, T_A, and T_B exerted on the proof mass M under acceleration a must satisfy following relation

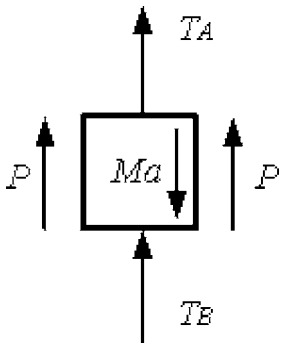

Fig. 5 Free body diagram of the proof mass M under acceleration a, subject to axial forces T_A and T_B from the microbeams A and B, and two reactions P, respectively, from the beams C and D.

$$T_A + T_B + 2P - Ma = 0. \tag{9}$$

Combining Eqs. (7), (8), and (9), the relation between P, T_A, and T_B of each microbeam in terms of acceleration can be obtained.

$$P = \frac{6MaI}{Al^2 + 12I}, \tag{10}$$

$$T_A = -T_B = Ma\left(\frac{1}{2} - \frac{6I}{Al^2 + 12I}\right). \tag{11}$$

When the axial loads in Eq. (11) due to 1-D acceleration are substituted into Eqs. (3), (4), and (5), the corresponding natural frequency shift for the stressed microbeams can be calculated. Thus, the relationship between acceleration and shifted natural frequency is established.

3.3 *Buckling Analysis for Proof Mass*

When a microbeam is buckled due to axial compression, its vibration frequency is zero, from Eqs. (3), (4), and (5). Thus, a buckling analysis is necessary to determine the maximum measurable acceleration for the compressed clamped-clamped microbeam. The allowable maximum axial compression $T_{B\,\max}$ occurring on microbeam B, as shown in Fig. 6, has to be less than the ultimate buckling load,[16] i.e.,

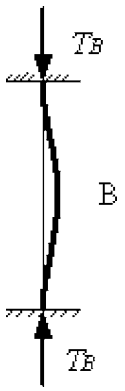

Fig. 6 Buckling of the clamped-clamped microbeam B subject to the axial load T_B under maximum acceleration.

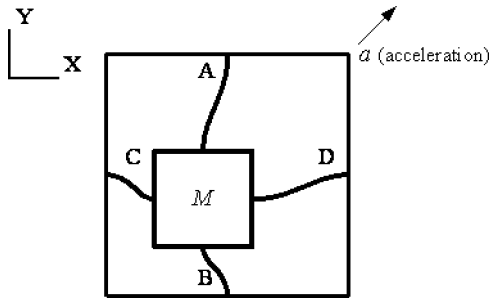

Fig. 7 The exaggerated deformation tendency of the microbeams under a planar acceleration *a*.

$$T_{B\max} \leqslant T_{cr} = \frac{4\pi^2 EI}{l^2}. \tag{12}$$

For determining the proof mass dimension, the bulking load limitation of Eqs. (11) and (12) are used. It is found that

$$T_{B\max} \cong \frac{M}{2} a_{\max}. \tag{13}$$

Thus, from Eqs. (12) and (13), the width L of proof mass M can be determined by specifying the length l of the microbeam and the maximum detectable acceleration $a_{\max}$.

3.4 *Calculation of 2-D Acceleration*

If the proposed structure design can decouple the signals from two axes coupled 2-D acceleration, the 1-D analytical model can be used to estimate a planar 2-D acceleration, shown in Fig. 7. Using Eqs. (3)–(5) and (11) to calculate the shifted natural frequencies for microbeams A, B, C, and D under axial loads, the x and y acceleration components a_x and a_y can be evaluated, respectively, and then the vector sum of these two components represents the planar acceleration a.

Table 1 Geometry parameters and mechanical properties in simulations.

Material	Ni
Dimension and property	
Length of the microbeam l (μm)	1000
Width of the microbeam w (μm)	5
Thickness of the beam and the proof mass h (μm)	20
First mode natural frequency f_o (kHz) of theclamped-clamped microbeam	25.107
Assigned maximum detectable acceleration (G)	10
Young's modulus E (GPa)	210
Mass density ρ (kg/m^3)	8800
Mass of the proof mass M (kg)	3.521×10^{-5}
Width of the proof mass L (μm)	14144.9

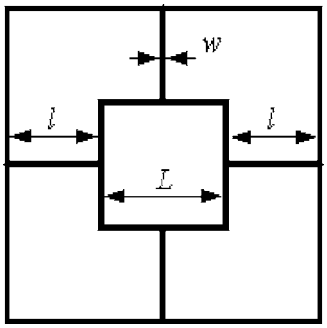

Fig. 8 The characteristic dimension of the accelerometer; the thickness of the proof mass and that of the microbeam are identical, indicated by *h* as shown in Fig. 1(b).

4 Simulation

The material properties of nickel and the geometry parameters of the microaccelerometer listed in Table 1 are used for analytical and FEA simulation. Figure 8 shows that the characteristic dimension L is the width of the square proof mass, while l and w are the length and the width of the microbeam, respectively. The analytical simulation results are shown in Fig. 9, and the symbols Ta, Ca, Da, Tf, Cf, and Df are explained in Table 2, in which the capital letters T and C respectively represent the frequency shift due to tension and compression, D is the frequency difference between these two frequency shifts, and the index a and f represent the results from analytical simulation and finite element analysis, respectively. The conditions for analytical or FEA simulations are listed in Table 3.

4.1 *1-D Analytical Simulation*

Figure 9 shows that the natural frequency shifts of microbeams under tension and compression are all quite linear with respect to the applied accelerations below 8 G, and the detecting sensitivity of Da is about 2400 Hz/G. By buck-

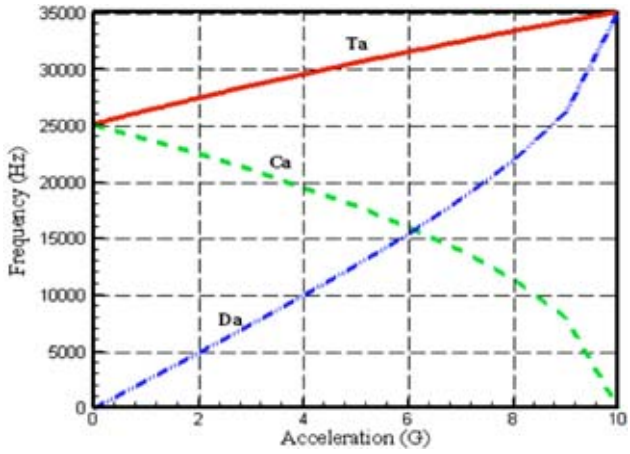

Fig. 9 The frequency shift of the microbeam of the proposed accelerometer at the F1-8 condition.

Table 2 Symbols used in the simulation results.

Simulation object	Symbol for analytical simulation	Symbols for FEA simulation
Natural frequency shift due to tension	Ta	Tf
Natural frequency shift due to compression	Ca	Cf
Difference of two above natural frequencies shifts	Da=Ta−Ca	Df=Tf−Cf

ling analysis, the microbeam subject to axial compression buckles at 10 G, and the corresponding resonant frequency becomes zero; thus the difference of the frequency shift increases abruptly at 10 G.

4.2 *Finite Element Analysis*

To realize the dynamic effect of the suspended proof mass, the inertia effect of the microbeam, and the structural cross talk, which are ignored in the analytical model, the FEA software ANSYS® is employed to verify the analytical results. FEA elements shell 63 and beam 4 are respectively adopted to depict the behaviors of the proof mass in acceleration detecting and the microbeams in natural frequency shifting, respectively. The imposed boundary condition on the position of the microbeam connected to the anchor frame is clamped and stationary. The boundary condition on the other end of the microbeam connected to the proof mass is a movable clamped end, and only translations along x, y, and z directions are allowed. Through static and prestressed modal analysis of FEA, the natural frequency shift of the microbeam responding to the acceleration is obtained.

In Table 3, the condition F1-8 means an external 1-D acceleration from 0 to 8 G in the y direction with an increment of 1 G in simulations, and the case F2-8 means an external 2-D acceleration comprised by a y-directional acceleration changing from 0 to 8 G by increments of 1 G in the y direction and a constant acceleration of 8 G in the x direction. To verify the capability of the structure to decouple a planar 2-D acceleration into two independent components a_x and a_y and validate the 1-D analytical model to evaluate the acceleration components, both analytical model and FEA simulations are performed for cases F1-8 and F2-8.

Table 3 Analytical and FEA simulation conditions.

Simulation conditions	Acc. dim.	Direction			
			y direction (G)		
		x direction (G)	Start	End	Inc
F1-8	1-D acceleration	0	0	8	1
F2-8	2-D acceleration	8	0	8	1

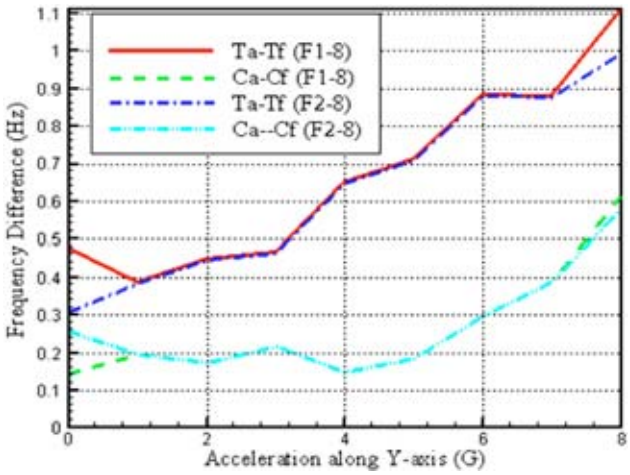

Fig. 10 The frequency shift difference between the analytical model and FEA at F1-8 and F2-8 conditions.

The deviation of simulation results between the analytical model and FEA is shown in Fig. 10. The solid line Ta-Tf (F1-8) in Fig. 10 is less than 1.1 Hz, indicating that the mass of microbeam ignored in the analytical model causes little deviation to the FEA result. On the other side, the dash-dot line Ta-Tf (F2-8) is less than 1 Hz, meaning that there is little deviation when using the 1-D derived model to do a 2-D simulation. Lines Ca-Cf (F1-8) and Ca-Cf (F2-8) also have the same results. In addition, the maximum shrinkage of microbeam with length 1000 μm before buckling is less than 0.007 μm, as shown in Fig. 10. It indicates that not only the cross talk of the proposed microaccelerometer is very small and negligible, but also the assumption of the clamped-clamped boundary condition in the analytical model has very little influence on the simulation result. The result verifies that the derived 1-D analytical model is able to estimate two independent acceleration components of a 2-D acceleration, decoupled by the proposed structure.

Table 4 Experimental data in Ref. 6.

Material	Polysilicon
Young's modulus E (GPa)	100
Mass density ρ (kg/m^3)	2300
Proof mass (mg)	1.45
Effective proof mass (mg) (due to eight constraint bridges)	0.4186
Dimension of microbridge (μm)	Length l: 250 Width w: 100 Thickness h: 1.6
Maximum detectable acceleration	1050 G
Natural frequency (kHz)	173
Sensitivity (Hz/G)	160

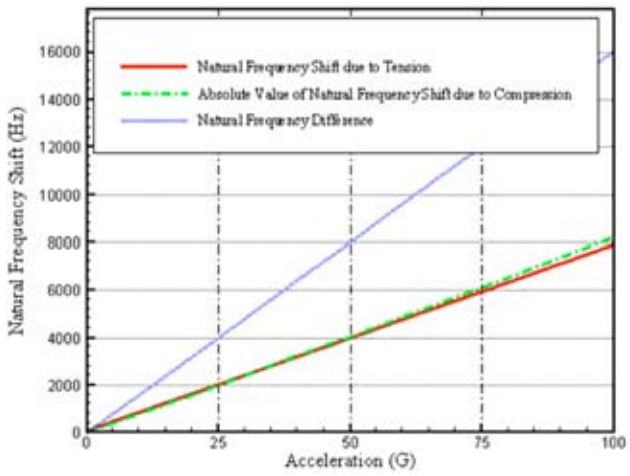

Fig. 11 Frequency evaluation of the DFSM[6] using the derived model; the sensitivity is 160 Hz/G.

5 Comparison with Previous Design

The experimental data listed in Table 4 from conventional DFSM microbridge design[6] are used to verify our analytical model. By substituting the material properties and geometrical parameters in Table 4 into our analytical model, the natural frequency shift under different accelerations can be obtained, as shown in Fig. 11. It shows that the calculated sensitivity, natural frequency difference of 160 Hz/G, agrees with the experimental results well, which further verifies our analytical model.

The calculation result also shows that the constraint bridges used to alleviate the displacement in Z directional acceleration, e.g., gravitation for the proof mass of the DFSM, also reduces the inertia effect of the proof mass from 1.45 to 0.4186 mg. However, in our proposed HAR microbeam design, the constraint microbridges are no longer needed; the effective proof mass will not be degenerated. In addition, the exciting and sensing electrodes are placed at two sides of microbeams instead of placing them on the substrate beneath the microbridge,[6] thus the capacitor area can be enlarged.

Table 5 Performance comparison between DFSM design[6] and the current design.

	Results of DFSM	Current design
Capacitor area	$1/3\times250\times100$ μm^2	250×100 μm^2
Structural rigidity (displacement in z direction at 1 G)	1 μm	0.507×10^{-3} μm
Sensitivity	160 Hz/G	555 Hz/G

To identify the enhancement of the proposed design, Table 5 compares the performance between the current design having a microbeam with dimensions of 250 μm long, 1.6 μm wide, and 100 μm thick, and the previous DFSM design having a microbridge with dimensions of 250 μm long, 100 μm wide, and 1.6 μm thick,[6] by using the same proof mass of 1.45 mg. It can be found that the capacitor area is three times larger, and the sensitivity of the proposed 2-D frequency-shift microaccelerometer with HAR resonant microbeams is 3.46 times higher than that of

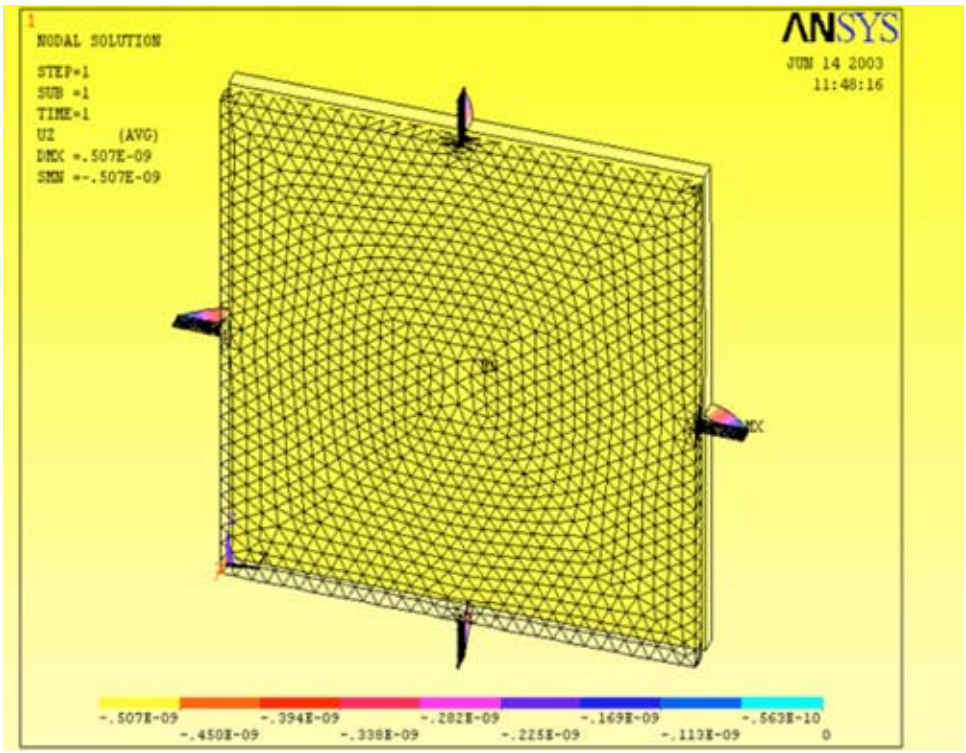

Fig. 12 The FEA simulation shows that the maximum z-directional displacement of the proof mass under 1G is about 0.507×10^{-9} m.

DFSM. Also, the displacement of proof mass due to z directional gravitation can be reduced from 1 μm to 0.507 $\times 10^{-3}$ μm, as shown in Fig. 12. It is evident that the proposed HAR microbeam design is effective in enhancing sensitivity and rigidity over the conventional constraint bridges design.

6 Conclusion

A HAR 2-D resonant microbeam accelerometer is proposed and analyzed. The simulation shows that the proposed structure is able to decouple a planar 2-D acceleration into two independent acceleration components, and the established analytical model is able to evaluate 1-D acceleration. FEA for 1-D and 2-D acceleration simulations are also performed to validate this analytical model, and the agreement between the analytical results and FEA simulation implies not only that the cross talk is negligible, but also the assumed fixed boundary condition influences the simulation result very little, meaning that the proposed structure is able to decouple a 2-D acceleration, and the derived 1-D analytical model therefore can be used to evaluate 2-D acceleration. In addition, the experimental results from the conventional microbridge design further verify the accuracy of the current model. From our simulation results, the proposed 2-D resonant microbeam accelerometer is more sensitive and also more rigid than the conventional constraint bridge design. It also reveals that the dimension arrangement has a direct influence on natural frequency shifting as well as the detecting sensitivity. Hence, the dimensions of the proof mass and the microbeams can be further optimized.

Acknowledgments

This paper is dedicated to Kan-Ping Chin, who was the first author's adviser and initiated this research. Unfortunately, Chin passed away on 8 February 2002 (1960-2002) due to pneumonia. The authors would like to thank S. C. Chang for his valuable suggestions on this research. Financial supports from the National Science Council of the Republic of China (contract number NSC88-2218-E-009-007) and the Materials Research and Development Center of CSIST (contract number BV89H14P) are acknowledged. The staff at the Nano Facility Center of National Chiao Tung University is also appreciated for providing technical assistance.

References

1. A. A. Seshia, M. Palaniapan, T. A. Roessig, R. T. Howe, R. W. Gooch, T. R. Schimert, and S. Montague, "A vacuum packaged surface micromachined resonant accelerometer," *J. Microelectromech. Syst.* **11**(6), 784–793 (2002).
2. M. Aikele, K. Bauer, W. Ficker, F. Neubauer, U. Prechtel, J. Schalk, and H. Seidel, "Resonant accelerometer with self-test," *Sens. Actuators, A* **92**, 161–167 (2001).
3. T. A. Roessig, R. T. Howe, A. P. Pisano, and J. H. Smith, "Surface-micromachined resonant accelerometer," *Transducer'97*, pp. 859–862 (1997).
4. P. Ohlckers, R. Holm, H. Jakobsen, T. Kvisteroy, G. Kittilsland, A. Larsen, M. Nese, S. M. Nilsen, and A. Ferber, "An integrated resonant accelerometer microsystem for automotive applications," *Sens. Actuators, A* **66**, 99–104 (1998).
5. D. W. Burns, R. D. Horning, W. R. Herb, J. D. Zook, and H. Guckel, "Sealed-cavity resonant microbeam accelerometer," *Sens. Actuators, A* **53**, 249–255 (1996).
6. S. C. Chang, M. W. Putty, D. B. Hicks, and C. H. Li, "Resonant-bridge two-axis microaccelerometer," *Sens. Actuators, A* **21–23**, 342–345 (1990).
7. O. Tabata and R. Yamamoto, "Two-axis detection resonant accelerometer based on rigidity change," *Sens. Actuators, A* **75**, 53–59 (1999).
8. S. Sung, J. G. Lee, B. Lee, and T. Kang, "Design and performance test of an oscillation loop for a MEMS resonant accelerometer," *J. Micromech. Microeng.* **13**(2), 246–253 (2003).
9. A. M. Hynes, H. Ashraf, J. K. Bhardwaj, J. Hopkins, I. Johnston, and J. N. Shepherd, "Recent advances in silicon etching for MEMS using the ASE™ process," *Sens. Actuators, A* **74**, 13–17 (1999).
10. C. Burbaum, J. Mohr, and P. Bley, "Fabrication of capacitive acceleration sensors by the LIGA technique," *Sens. Actuators, A* **25–27**, 559–563 (1991).
11. D. H. Hwang, Y. C. Lo, and K. P. Chin, "Development of a systematic recipe set for processing SU8-5 photoresist," *Proc. SPIE* **4592**, 131–139 (2001).
12. H. Lorenz, M. Despont, N. Fahrni, N. LaBianca, P. Renaud, and P. Vettiger, "SU-8: a low cost negative resist for MEMS," *J. Micromech. Microeng.* **7**(3), 121–124 (1997).
13. H. Lorenz, M. Despont, N. Fahrni, J. Brugger, P. Vettiger, and P. Renaud, "High-aspect-ratio, ultrathick, negative-tone near-UV photoresist and its applications for MEMS," *Sens. Actuators, A* **64**, 33–39 (1998).
14. S. A. D. Dimarogonas and S. Haddad, *Vibration For Engineer*, Prentice-Hall, Englewood Cliffs, NJ (1992).
15. W. T. Thomson, *Theory of Vibration with Application*, 3rd ed., Prentice-Hall, Englewood Cliffs, NJ (1988).
16. F. P. Beer and E. R. Johnston, Jr., *Mechanics of Materials*, McGraw-Hill Ryerson Limited, New York (1987).

Deng-Huei Hwang received his BS and MS degrees in mechanical engineering from National Chiao Tung University, HsinChu, Taiwan, in 1991 and 1993, respectively. His research activity mainly involves design of structure of MEMS inertial sensors, MEMS inertial sensor applications, UV-LIGA-like fabrication processes, and control systems. He is now a research and development engineer of NeoStones MicroFabrication Corporation in Taiwan, and focuses on designs of microaccelerometers and microgyros.

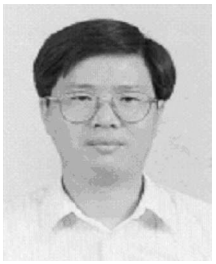

Kan-Ping Chin received the BS degree in mechanical engineering from National Taiwan University in 1982, and the MS and PhD degrees from Massachusetts Institute of Technology in 1988 and 1991, respectively. He was an associate professor at National Chiao-Tung University in Taiwan. His research interests included control of servomotors and microelectromechanical systems (micromotors). He passed away on 8 February 2002 due to pneumonia.

Yi-Chung Lo received the BS degree from the Department of Mechanical Engineering at National Chiao-Tung University, Taiwan, in 1986, and the MS and PhD degrees in materials science from the National Taiwan University in 1988 and 1992, respectively. From 1993 to 1994 he was with the Lawrence Berkeley Laboratory, Material Science Division as a postdoctoral research associate. In 1995, he was a visiting scientist at the Institut für Mikrostrukturtechnik (IMT) of Kernforschungzentrum Karlsruhe (KfK) in the Deep X-Ray Lithography (DXRL) group of LIGA technology. Since 1996 he has been an associate research scientist at National Synchrotron Radiation Research Center (NSRRC), Taiwan, in the development of x-ray micromachining and LIGA-like processes. In 1997, he also held a part-time professorship contract as an associate professor with the mechanical engineering department at National Chiao-Tung University, Taiwan. His research interest and activities include design, modeling, and microfabrication of MEMS microstructures, microsensors, and microactuators.

Wensyang Hsu received the BS degree in mechanical engineering from National Chiao Tung University in Taiwan in 1985, then the MS and PhD degrees in mechanical engineering from the University of California at Berkeley in 1989 and 1992, respectively. He joined National Chiao Tung University in 1992. Currently, he is a professor in Department of Mechanical Engineering. His research interests in microelectromechanical systems include design and fabrication of microstructures, microsensors, and microactuators.